Towards Lightweight Structure: Coupling Topology Optimization with Non-Planar 3D Concrete Printing

Yuxin Lin, Alireza Bayramvand, Mania Aghaei Meibodi[1]

DART Laboratory, Taubman College of Architecture and Urban Planning
University of Michigan, Ann Arbor, MI 48109, USA

Abstract. This study explores the integration of Topology Optimization (TO) with non-planar 3D concrete printing (NP-3DCP) to address environmental and material efficiency challenges in construction. We present a novel approach leveraging robotic NP-3DCP for creating lightweight, structurally optimized architectural components, specifically focusing on load-bearing walls. The advantages of this approach were demonstrated through the manufacturing of two prototypes, Shell Wall and Branch Wall, showcasing significant material savings and reduced carbon footprint without compromising structural integrity. Our methodology encompasses the generation of a non-planar printpath, material extrusion control for variable layer height, and the integration of rebar and thermal insulation within the casting process. The results showcase the potential of this approach in producing complex geometries with improved environmental performance, suggesting a promising direction for the future of sustainable concrete construction.

Keywords: Lightweight structure · Topology optimization · Robotic 3D concrete printing · Non-planar printpath

1 Introduction

The increasing urban population intensifies the need for housing and infrastructure. Reinforced concrete is important to meeting this rising demand, due to its strength, durability, affordability, and capability to create long-span structures [1]. Yet, the inefficient practices in concrete construction have led to excessive use of concrete, consequently amplifying cement production, which intensifies the scarcity of sand and accounts for over 8% of the global CO2 emissions [2]. There is a

---

[1] Mania Aghaei Meibodi (✉)
DART Laboratory, University of Michigan, Ann Arbor, MI 48109, USA
e-mail: meibodi@umich.edu

pressing need to adopt material optimization strategies aimed at developing lightweight load-bearing concrete structures that can minimize material consumption while ensuring structural integrity and consequently reduce the carbon footprint. Topology Optimization (TO) is a technique that can achieve lightweight designs by optimally distributing material within a given design space, systematically eliminating structurally inefficient areas [3]. TO methods often results in forms entailing complex geometries characterized by extreme overhangs, ribbed geometries, and branches with varying sections and angles. Producing these intricate geometries presents a challenge when using traditional concrete production techniques, primarily due to the increased complexity of the required formwork and the costs associated with fabricating non-standard formwork, which can consume over half of the structure's total budget [4].

The combination of 3D concrete printing (3DCP) with TO is a promising field of research as it has the potential to address the material efficiency with reduced cost for fabrication. Because 3DCP precisely places material only where it is needed. Previous studies have shown that coupling 3D printing (3DP) with structural and material optimization strategies can significantly reduce environmental impact [5], and is estimated to minimize the environmental footprint of construction practice by about 50% [6]. Nonetheless, there are challenges that arise in the production of complex geometries using 3DCP. The most prevalent technique in 3DCP involves the planar deposition of material in a linear, horizontal manner. This approach, when applied to the manufacturing of complex geometries, results in undesired "staircase effect," (Fig. 1) where each layer is only partially supported by the one beneath it, impacting the overall buildability [7].

Non-planar 3D concrete printing (NP-3DCP) is a promising method for manufacturing complex parts as it enables variations in orientation and layer height (Fig. 1). This method is critical for accurately contouring the profile of intricate designs enhancing the geometric fidelity of the 3D printed complex parts. NP-3DCP diverges from traditional layer-by-layer, horizontal deposition, by using non-planar printpath that follows the exact contour of the part. To deposit concrete along the contour of the part in a non-planar fashion, it is essential to use a 6-axis robotic arm.

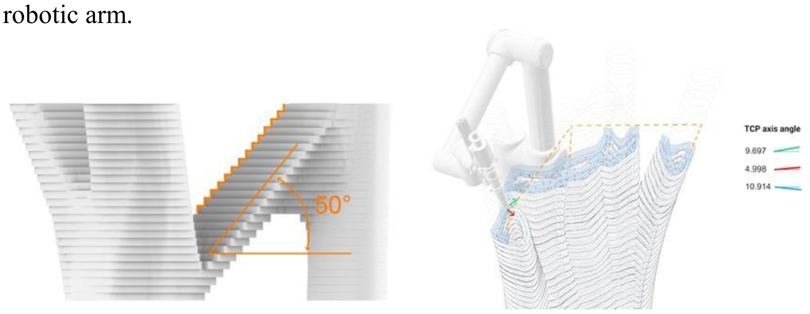

Fig. 1 The planar material deposition (left) results in "staircase effect" when printing overhanging structures which affects buildability. 3D simulation of the non-planar printpath and the material deposition process (Right)

2 Robotic Non-planar 3D Concrete Printing Strategies

Non-planar Printpath required for Complex Geometries

Non-planar printpath (NP-printpath) guides the movement of the printhead in three dimensions within a single layer. Instead of strictly being confined to horizontal planar layers, the printhead is allowed a higher degree of freedom to vary in X, Y, and Z axes simultaneously while changing the Tool Center Point (TCP) orientation. This approach allows the creation of curved, sloped or angled surfaces when 3D printing, closely following the object's 3D geometry. This method effectively alleviates the "staircase effect" by depositing a new layer precisely on the previous one, facilitating the fabrication of a wide variety of topology-optimized forms.

The need for Precise Material Deposition in NP-3DCP

A NP-printpath is accompanied by a variable layer height and orientation changes responding to the complex geometric features of the 3D printed object [8]. Thus, the precise control of variable material extrusion rate is essential to match the varying layer height [9, 10]. Similar to planar 3DCP, and perhaps even more crucially, achieving precision in NP-3DCP for complex geometry demands the deposition of an optimal amount of material at each layer. This not only impacts the buildability and structural integrity of the printed parts but also significantly enhances the surface finishing. The basic equation for 3DCP has been defined as:

$$H * W = F / V \tag{1.1}$$

Here H is layer height; W is extrudate material width; F is material flow rate based on pump speed; and V is nozzle travel speed [11]. The extruded material width (W) and the material flow rate (F) were kept constant in this paper; Thus, the variable layer height (H) depends on the nozzle travel speed (V). A smaller H requires a faster V, and vice versa. The method involves calculating the H by measuring each point on the current printpath and the nearest point on the preceding path, then subsequently using H to adjust the V during the printing process.

3 Topology Optimization and Printpath Generation Methods

Optimization Strategies and Geometric Post-processing Techniques

The main objectives in applying the TO method on concrete elements are reducing the weight of the component by optimizing material usage and enhancing performance capabilities [12]. Shell Wall was generated from two supports and two loads. Multiple iterations of optimization were followed by mesh reconstruction and simplification; the resulting structural ribs represent the wall's optimal material distribution. Subsequently, ribbed structures from TO were utilized as a frame to generate the minimal surface representing the in-between non-loading bearing area (Fig. 2). The Branch Wall design includes four support locations and six load-bearing points, resulting in a branched structure (Fig. 2). Further refinement was necessary through mesh relaxation and subdivision to enhance mesh quality. Additionally, the resulting form was modified to have a hollow structure with a wall thickness of 20mm, equivalent to the filament width used in the printing process. This modification created voids within the structure, allowing it to serve as formwork for concrete casting. Additionally, these voids served as spaces to host steel rebars and insulation.

Fig. 2 Topology optimization process and geometric post-processing: Shell Wall (left) and Branch Wall (right)

NP-printpath Generation in relation to Complex Geometries

Methods of Generating NP-printpath in Shell Wall:
The central axis of the structural ribs is discretized into segments with a uniform length. At each segmentation point, planes are orthogonally aligned along the central axis. The printpath for the ribs is determined by the intersection of these planes with the topology-optimized structural ribs. The printpath corresponding to each rib is then interconnected using planar contours, following the curvature of the minimal surface of the optimized geometry (Fig. 3). The printhead's orientation aligns tangent to the central axis and the planar contours for each corresponding layers.

Methods of Generating NP-printpath in Branch Wall:
Branch Wall features four overhanging branches so it is critical to identify the branching moments within the geometry. First, we slice the TO generated geometry with a horizontal plane that moves from the bottom upwards. This process generated a series of intersected curves. For each curve, the central point was determined and sequentially connected vertically, forming the reeb graph that represents the geometry's topology. Through the reeb graph [13], critical points can be detected that are essential for segmenting the original geometry into distinct branches. Then we set paths at the local minima (gray mark) and local maxima (black mark), as well as the desired path in the middle on each branch. The final printpath was then generated by interpolating these pre-set paths (Fig. 3). The final step involves determining the orientation of the nozzle, which is accomplished by

initially dividing each layer with division points every 50mm. Subsequently, these division points are projected onto the previous contour using the shortest route. The vector originating at each division point and pointing towards its projection on the previous contour is regarded as the printing direction of the nozzle.

Bifurcation requires lead-in and lead-out strategies within the printpath design to address the challenge of navigating "islands" — disconnected sections within the branching areas that necessitate a robotic mechanism to navigate between them without depositing excessive material. The lead-in method starts the extruder 20 mm above each printpath, descends, and simultaneously extrudes material while avoiding collision with an already 3D-printed structure. The lead-out method stops material flow using a pinch valve at each printpath's endpoint and retraces a portion of the already printed path. Then the printhead elevates and moves to the next island. This technique effectively eliminates any residual material on the nozzle, ensuring a more precise printing process.

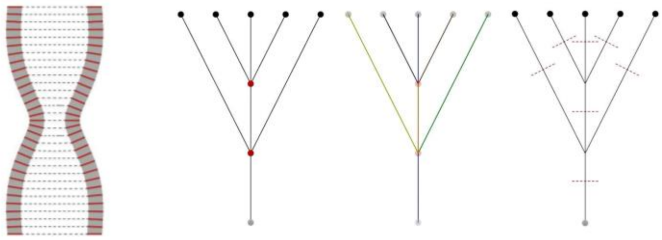

Fig. 3 The non-planar printpath generation process of Shell Wall (left) and Branch Wall (right)

4 Method for Remapping Extrusion Parameters to Complex 3D Geometry

Material Exploration for Pumpability and Extrudability to Achieve a Stable Flow Rate

Robotic 1-component (1k) system was utilized in this research and the mortar used in this study consists of fine sand, ordinary Portland cement, fly ash, water, and superplasticizer. Components ratios were fine-tuned through testing various ratios of water-reducer (superplasticizer, in this context) to identify the optimal viscosity for 1) ensuring pumpability – a consistent material flow without separation or loss of consistency during pumping and 2) achieving extrudability – the ability of the mix to be extruded from the nozzle and maintain its shape upon deposition [14].

To guarantee the homogeneity of the material, the base mortar was thoroughly mixed for 12 minutes and then divided into four separate batches. Varying Superplasticizer-Binder Ratio ranging from 0.14% to 0.26%, were added to each batch, and followed by mixing the material for another 2 minutes. A funnel viscosity tool was used to visually assess the quality of the mixed concrete mortar. The exact mortar ratios for each batch as well as the measured results from the conducted tests and experiments are described in Table 1. Based on these findings, the optimal viscosity was concluded to be when the Superplasticizer-Binder Ratio was maintained at 0.18%.

No.	Water-Cement Ratio	Water-Binder Ratio	Superplasticizer-Binder Ratio	Pump ability	Extrudability	Shape retainability after deposition
01	0.553	0.25	0.14%	Hard	Separate	Good
02	0.553	0.25	0.18%	Good	Consistent	Good
03	0.553	0.25	0.22%	Good	Fair	Fair
04	0.553	0.25	0.26%	Fluid	Fluid	Bad

Table 1 Data of material explorations through different batches for pumpability, extrudability, and shape retainability after deposition

Deposition Calibration Experiment for Variable Height Through Parallel Testing

The quality of the material deposition is directly influenced by the relation between the layer height and printing nozzle diameter (ND). Using layer heights smaller than the ND helps in preventing defects and enhancing the filament overlap, as it ensures layers are more effectively pressed. However, setting the layer height too small can lead to over-extrusion issues. Conversely, selecting layer heights larger than the nozzle diameter can lead to increased voids and suboptimal filament overlap [15]. The presented research utilized a circular nozzle with 20mm in diameter and the average height per layer was maintained at 0.5 time ND with maximum layer height below 0.83 times ND, which was showcased in the literature to have better layer bonding and buildability [15, 16].

12 experiments were conducted to evaluate the material behavior in relation to the robotic 3D printing settings, the results and setup for these experiments are described in Table 2. The printing nozzle diameter used measured 18mm, two layer heights were tested 9mm (50% ND) and 13.5mm (75% ND), in combination with six printing speeds to identify the optimal speed for each layer height. An optimal nozzle travel speed has been visually assessed by evaluating the occurrence of material over-extrusion and under-extrusion. The results from the experiments demonstrated that 32mm/s and 23mm/s nozzle travel speeds performed well when combined with 9mm and 13.5mm layer heights, respectively.

H	9mm						13.5mm					
V (mm/s)	20	26	32	38	44	50	13	18	23	28	33	38
W (mm)	36	29	24.5	20	18.5	17.2	34.5	27.3	23.8	19	16	13

Visual Assessment					Collapsed						

Table 2 The top views of 12 printed samples with 2 different layer heights and corresponding 6 different nozzle travel speeds

Adjusting Nozzle Travel Speed through Parameters derived from NP-printpath

The findings presented in Table 2 aligns with Equation 1.1, demonstrating that when under optimal extrusion situations, the relationship between layer height and nozzle travel speed is an inverse relation, provided that the filament width and material flow rate remain constant. Speed can be remapped inversely proportional to different layer height through Equation 1.1.

Manipulating the extrusion rate is achieved by altering the robot's nozzle travel speed that can be calculated in relation to the changing in layer height at each point. As described before, each layer of printpath has been uniformly sampled with points and a vector representing the shortest distance was used to set the printhead's orientation (Fig. 4). Here, layer height is determined through measuring the shortest distance. This value will serve as input H for Equation 1 and the V will be calculated based on that.

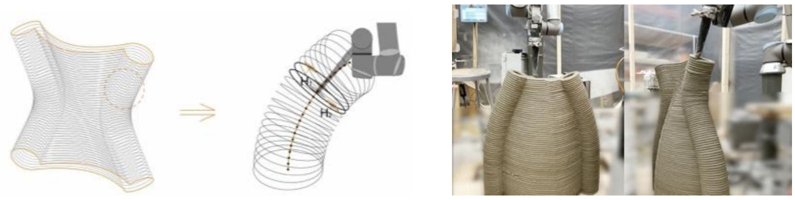

Fig. 4 Nozzle travel speed based on changing layer heights (left) and toolhead orientations (right)

5 Method for Rebar and Insulation Integration with Casting

Sequential Integration of Rebar and Casting through Pauses: Shell Wall

Rebar integration along with NP-3DCP is essential for creating lightweight structures that possess the required strength to counter tensile loads. The ribbed geometry in Shell Wall, a common characteristic of structurally optimized forms, facilitates the effective incorporation of longitudinal reinforcement. The ribs are post rationalized to have a hollow cross section that hosts the rebars. Due to the complex geometries the rebars needed to be discretized into smaller sections that were sequentially manually integrated into the form, which was followed by the manual casting of concrete. This manual part of the process required the halting of the 3DP process at various stages of the manufacturing process as shown in Fig. 5.

Simultaneous 3DCP and Set-On-Demand Casting for Overhangs: Branch Wall
A similar approach was applied to construct the first half of the Branch Wall in which ribs and membrane areas are connected. Nonetheless, challenges arose for the top part when dealing with overhanging branches—particularly at angles greater than 75 degrees. The gravitational forces would often cause the freshly printed parts to slump, leading to collapse immediately after the deposition of the freshly printed material. To address this, a method was introduced to manually cast fast-setting concrete after the rebar reinforcement is successfully integrated (Fig. 5). The casting intervals were set every 25 to 50mm of freshly 3D printed material based on the angle of the overhang.

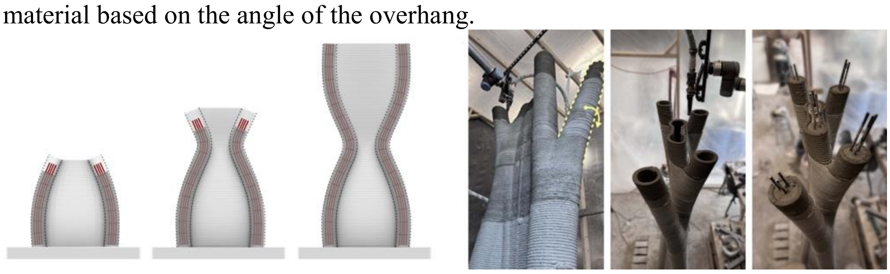

Fig. 5 Sequential integration of rebar and insulation with concrete casting (left). The collapse due to self-weight requires simultaneous 3DCP and set-on-demand casting (right)

6 Results and Discussion

Shell Wall and Branch Wall (Fig. 6) can be actualized for a wide range of topologically complex features in construction scale, the successful fabrication them demonstrates the potential of coupling Topology Optimization and non-planar 3D concrete printing to create ultra-lightweight walls. Shell Wall, having a width ranging from 490mm at the ends to 140mm in the middle and a height of 1.5m, is a ribbed structure with a doubly curved membrane/surface in between. It weighs only 160 kilograms, showcasing the potential for zero waste production since no additional materials, such as scaffolding, were utilized. Meanwhile, Branch Wall, measuring 1.2m in width and 2m in height, features more geometric complexity such as multiple intersecting branches, overhanging structural ribs, and ultra-thin membranes. It weighs 367 kilograms, demonstrating a 68% reduction in material use compared to a standard load-bearing concrete wall with similar dimensions and load-bearing capacity.

Variable material extrusion rate achieved by adjusting the nozzle travel speed, was critical for the accurate fabrication complex geometrical features of the presented prototypes. The nozzle travel speed was determined based on changing layer height. Nevertheless, fluctuating flow rates were observed due to the increase of material viscosity through time during printing, necessitating manual adjustments to the nozzle speed based on visual inspections. Future research should focus on the development of a closed loop system capable of providing real-time feedback for immediate and accurate process adjustments.

Rebar reinforcement was successfully incorporated within the 150 mm tubular rib structural components of the Shell Wall, followed by concrete casting. For Branch Wall, the use of fast-setting concrete enabled the printing of branches with a diameter of 300mm and lengths of up to 790mm, while supporting overhangs of up to 70 degrees. Moreover, the integration of 50mm thick XPS insulation into the double-layered sections improved the walls' thermal performance. Challenges such as shape deformation during printing and casting were observed due to the material setting time and hydrostatic pressure exerted by the casted concrete. Further investigation is needed in the geometric fidelity of the proposed method through live data collection.

Fig. 6 3D concrete printed topology-optimized walls: Shell Wall (left) and Branch Wall (right)

7 Conclusion

The research provided evidence that the integration of TO with robotic NP-3DCP presents a viable solution for constructing lightweight, and structurally optimized architectural elements. Non-planar printpath and variable material deposition are necessary for successful 3DCP of complex geometries. The fabrication of the Shell Wall and Branch Wall prototypes illustrates the potential of this method in reducing material usage by up to 68% compared to traditional construction methods, thereby demonstrating the potential of this method in achieving a lower carbon footprint, offering a more sustainable alternative to traditional approaches. Further research needs to address challenges such as fluctuating flow rates, material deformation, real-time printpath adjustment and live 3DCP data synchronization to ensure geometric fidelity.

8 References

1. Belaïd F. How does concrete and cement industry transformation contribute to mitigating climate change challenges? Resour Conserv Recycl Adv [Internet]. 2022;15(200084):200084. Available from: http://dx.doi.org/10.1016/j.rcradv.2022.200084
2. Van Damme H. Concrete material science: Past, present, and future innovations. Cem Concr Re [Internet]. 2018;112:5 – 24. Available from: http://dx.doi.org/10.1016/j.cemconres.2018.05.002
3. Bi M, Tran P, Xia L, Ma G, Xie YM. Topology optimization for 3D concrete printing with various manufacturing constraints. Addit Manuf [Internet]. 2022;57(102982):102982. Available from: http://dx.doi.org/10.1016/j.addma.2022.102982
4. García de Soto B, Agustí-Juan I, Hunhevicz J, Joss S, Graser K, Habert G, et al. Productivity of digital fabrication in construction: Cost and time analysis of a robotically built wall. Autom Constr [Internet]. 2018;92:297 – 311. Available from: http://dx.doi.org/10.1016/j.autcon.2018.04.004
5. Vantyghem G, De Corte W, Shakour E, Amir O. 3D printing of a post-tensioned concrete girder designed by topology optimization. Autom Constr [Internet]. 2020;112(103084):103084. Available from: http://dx.doi.org/10.1016/j.autcon.2020.103084
6. Biernacki JJ, Bullard JW, Sant G, Banthia N, Brown K, Glasser FP, et al. Cements in the 21st century: Challenges, perspectives, and opportunities. J Am Ceram Soc [Internet]. 2017;100(7):2746 – 73. Available from: http://dx.doi.org/10.1111/jace.14948
7. Lao W, Li M, Tjahjowidodo T. Variable-geometry nozzle for surface quality enhancement in 3D concrete printing. Addit Manuf [Internet]. 2021;37(101638):101638. Available from: http://dx.doi.org/10.1016/j.addma.2020.101638
8. Mitropoulou I, Bernhard M, Dillenburger B. Print Paths Key-framing: Design for non-planar layered robotic FDM printing. In: Symposium on Computational Fabrication. New York, NY, USA: ACM; 2020.
9. Anton A, Yoo A, Bedarf P, Reiter L, Wangler T, Dillenburger B. Vertical Modulations. In: ACADIA proceedings. ACADIA; 2019.
10. Carneau P, Mesnil R, Roussel N, Baverel O. Additive manufacturing of cantilever - From masonry to concrete 3D printing. Autom Constr [Internet]. 2020;116(103184):103184. Available from: http://dx.doi.org/10.1016/j.autcon.2020.103184
11. Anton A, Reiter L, Wangler T, Frangez V, Flatt RJ, Dillenburger B. A 3D concrete printing prefabrication platform for bespoke columns. Autom Constr [Internet]. 2021;122(103467):103467. Available from: http://dx.doi.org/10.1016/j.autcon.2020.103467
12. Liu D, Zhang Z, Zhang X, Chen Z. 3D printing concrete structures: State of the art, challenges, and opportunities. Constr Build Mater [Internet]. 2023;405(133364):133364. Available from: http://dx.doi.org/10.1016/j.conbuildmat.2023.133364
13. Biasotti S, Giorgi D, Spagnuolo M, Falcidieno B. Reeb graphs for shape analysis and applications. Theor Comput Sci [Internet]. 2008;392(1 – 3):5 – 22. Available from: http://dx.doi.org/10.1016/j.tcs.2007.10.018
14. Yuan PF, Zhan Q, Wu H, Beh HS, Zhang L. Real-time toolpath planning and extrusion control (RTPEC) method for variable-width 3D concrete printing. J Build Eng [Internet]. 2022;46(103716):103716. Available from: http://dx.doi.org/10.1016/j.jobe.2021.103716
15. Nair SAO, Tripathi A, Neithalath N. Examining layer height effects on the flexural and fracture response of plain and fiber-reinforced 3D-printed beams. Cem Concr Compos [Internet]. 2021;124(104254):104254.
16. Lee H, Kim J-HJ, Moon J-H, Kim W-W, Seo E-A. Evaluation of the mechanical properties of a 3D-printed mortar. Materials (Basel) [Internet]. 2019;12(24):4104. Available from: http://dx.doi.org/10.3390/ma12244104